Monthly Notices
of the
ROYAL ASTRONOMICAL SOCIETY

MNRAS **453,** 1047–1061 (2015) doi:10.1093/mnras/stv1588

The new Milky Way satellites: alignment with the VPOS and predictions for proper motions and velocity dispersions

Marcel S. Pawlowski,[1]⋆ Stacy S. McGaugh[1] and Helmut Jerjen[2]

[1]*Department of Astronomy, Case Western Reserve University, 10900 Euclid Avenue, Cleveland, OH 44106, USA*
[2]*Research School of Astronomy and Astrophysics, Australian National University, Mt Stromlo Observatory, Cotter Rd., Weston ACT 2611, Australia*

Accepted 2015 July 13. Received 2015 July 6; in original form 2015 May 26

ABSTRACT

The evidence that stellar systems surrounding the Milky Way (MW) are distributed in a Vast Polar Structure (VPOS) may be observationally biased by satellites detected in surveys of the northern sky. The recent discoveries of more than a dozen new systems in the Southern hemisphere thus constitute a critical test of the VPOS phenomenon. We report that the new objects are located close to the original VPOS, with half of the sample having offsets less than 20 kpc. The positions of the new satellite galaxy candidates are so well aligned that the orientation of the revised best-fitting VPOS structure is preserved to within 9°and the VPOS flattening is almost unchanged (31 kpc height). Interestingly, the shortest distance of the VPOS plane from the MW centre is now only 2.5 kpc, indicating that the new discoveries balance out the VPOS at the Galactic centre. The vast majority of the MW satellites are thus consistent with sharing a similar orbital plane as the Magellanic Clouds, confirming a hypothesis proposed by Kunkel & Demers and Lynden-Bell almost 40 yr ago. We predict the absolute proper motions of the new objects assuming they orbit within the VPOS. Independent of the VPOS results, we also predict the velocity dispersions of the new systems under three distinct assumptions: that they (i) are dark matter free star clusters obeying Newtonian dynamics, (ii) are dwarf satellites lying on empirical scaling relations of galaxies in dark matter haloes and (iii) obey modified Newtonian dynamics.

Key words: Galaxy: halo – galaxies: dwarf – galaxies: kinematics and dynamics – Local Group – Magellanic Clouds.

1 INTRODUCTION

It has been known for almost 40 yr now that the satellite galaxies of the Milky Way (MW) preferentially lie along a great circle in the sky which passes almost through the Galactic poles. The MW satellites are thus distributed in a flattened, polar plane. From the beginning, it was noticed that this plane contains the Magellanic Clouds and follows the Magellanic Stream. Hence, Kunkel & Demers (1976) and Lynden-Bell (1976) termed this phenomenon the 'Magellanic plane'. As more MW satellites were discovered, e.g. Sextans and those dwarf galaxies in the footprint of the Sloan Digital Sky Survey (SDSS), they were found to lie close to this plane too (Kroupa, Theis & Boily 2005; Metz, Kroupa & Jerjen 2009).

With the inclusion of other types of MW halo objects, this plane was subsequently called the Vast Polar Structure (VPOS) of the MW (Pawlowski, Pflamm-Altenburg & Kroupa 2012). It was found that young halo globular clusters, which are hypothesized to have formed in external dwarf galaxies that were accreted into the Galactic potential well, follow the same polar distribution (Keller, Mackey & Da Costa 2012; Pawlowski et al. 2012). Even the stellar streams of some disrupting MW satellites (both galaxies and star clusters) have been found to align with the VPOS (Pawlowski et al. 2012; Pawlowski & Kroupa 2014). The orbital directions of the 11 classical satellites, deduced from their proper motions (PMs), further indicate that most satellites co-orbit in the plane. The VPOS is thus not only a spatial but also a rotating structure (Pawlowski & Kroupa 2013).

Kroupa et al. (2005) were the first to argue that the narrow, polar alignment of the 11 brightest 'classical' MW satellites is in conflict with the typical distribution of dark matter sub-haloes in Λ cold dark matter (ΛCDM). Whether the positional alignment of these 11 satellite galaxies is problematic for ΛCDM or not has been challenged since then (e.g. Deason et al. 2011; Libeskind et al. 2005, 2009; Wang, Frenk & Cooper 2013; Zentner et al. 2005). Taking into account the limitation of detecting satellite galaxies close to the Galactic plane, the significance of the planar arrangement of the 11 satellites is between 99.4 and 99.9 per cent (Pawlowski et al. 2014; Pawlowski & McGaugh 2014b). Due to minor anisotropies present in dark matter sub-halo systems around MW equivalents in

⋆ E-mail: marcel.pawlowski@case.edu

simulations, it has been found that the VPOS flattening alone can be reproduced by 0.5–6 per cent of ΛCDM systems (Wang et al. 2013; Pawlowski et al. 2014; Pawlowski & McGaugh 2014b). However, once the kinematic correlation is being taken into account, structures like the VPOS are extraordinarily rare in cosmological simulations (<0.1 per cent; Pawlowski et al. 2014; Pawlowski & McGaugh 2014b). Planar satellite arrangements sometimes occurring in the simulations tend to be transient features without aligned orbits (e.g. Gillet et al. 2015).

The significance of the VPOS can be tested with the help of additional satellite galaxies. In the data of the SDSS (York et al. 2000) 15 faint and ultrafaint satellite galaxies have been discovered between 2005 and 2010 (Willman et al. 2005a,b; Belokurov et al. 2006, 2007, 2008, 2009, 2010; Sakamoto & Hasegawa 2006; Zucker et al. 2006a,b; Walsh, Jerjen & Willman 2007; Grillmair 2009). These additional objects have supported the notion that the majority of MW satellites are part of a single halo structure: they independently define a polar plane which is closely aligned with the original disc of satellites (Kroupa et al. 2010). However, the VPOS results are based on the SDSS survey footprint, which covers the North Galactic Pole region and thus the SDSS satellites may be expected to lie close to the VPOS. The SDSS survey nevertheless provides additional constraints. Metz et al. (2009) noted a deficit of SDSS-discovered satellite galaxies away from the satellite plane at large Galactocentric distances. If the satellites discovered in the SDSS would be drawn from an isotropic distribution, the chance of them being oriented in a similarly narrow plane this closely aligned with that defined by the 11 classical satellites is small (Pawlowski, in preparation). In addition, even though the SDSS survey area was extended since data release 7, no new MW satellite galaxies were discovered outside of the VPOS (Pegasus III, recently discovered in SDSS DR10 data by Kim et al. 2015b, aligns well with the VPOS as will be shown later).

Recently, a number of new surveys began to operate, facilitating a wider search for MW satellites beyond the SDSS footprint. The Pan-STARRS1 survey covers three quarters of the entire sky ($\delta > -30^\circ$), with much of this area being far away from the VPOS and not covered by SDSS. Two new MW satellite objects have been discovered in this survey so far: the remote globular cluster PSO J174.0675-10.8774 (Laevens et al. 2014) also known as Crater (Belokurov et al. 2014), which happens to lie close to the VPOS (Pawlowski & Kroupa 2014), and the dwarf satellite Triangulum II (Laevens et al. 2015).

In recent months, the Stromlo Milky Way Satellite Survey (Jerjen 2010), the Dark Energy Survey (DES; The Dark Energy Survey Collaboration 2005) and the Survey of the Magellanic Stellar History (Olsen et al. 2014; PI: D. Nidever) have been revealing a series of new MW companions: two ultrafaint star clusters Kim 1 (Kim & Jerjen 2015a) and Kim 2 (Kim et al. 2015a), and two ultrafaint dwarf galaxies: Pegasus III (Kim et al. 2015b) and Hydra II (Martin et al. 2015). Two studies of the DES-Y1A1 survey data announced the discovery of seven (Bechtol et al. 2015, hereafter B15), respectively, eight (Koposov et al. 2015a) new objects, not counting Kim 2 (or Indus I), which has been already found earlier (Kim et al. 2015a). Furthermore, Kim & Jerjen (2015b) have discovered an additional object, Horologium II, in the same data set which apparently was overlooked previously. One of the objects discovered in the DES, Eri II, is most likely beyond the virial radius of the MW. Fundamental parameters for these new objects are compiled in Table 1. Fig. 1 shows their positions in relation to the MW, the previously known satellites and the Magellanic Stream in an all-sky plot.

Many of the new objects are candidate satellite galaxies although the distinction between star clusters and ultrafaint satellite galaxies based on their size and luminosity alone is becoming increasingly blurry. We therefore refrain from choosing a preferred name, but instead list all suggested names in Table 1. We will identify the objects by the abbreviations given in the first column, consisting of three letters and a roman numeral, except Kim 1 and 2, which have been unambiguously classified as star clusters.

The alignment of the satellite galaxies in a common structure indicates that they might be dynamically associated, sharing similar orbits. This assumption allows us to predict their PMs (Lynden-Bell & Lynden-Bell 1995; Pawlowski & Kroupa 2013), measurement of which then provides a crucial test of whether the assumed association is real. The existence of the VPOS and the preferential alignment of streams with this structure indicates such a dynamical association of its constituents. The fact that the 11 classical MW satellites already have PM measurements which show that most of them indeed (co-)orbit in the VPOS further supports this interpretation. The PMs of the new MW satellite objects can thus be predicted in an entirely empirical way (Pawlowski & Kroupa 2013). This prediction is based solely on the current spatial distribution of the MW satellites and does not require an assumption of a specific MW potential or underlying type of dynamics. Confidence in the method can be drawn from the finding that more precise PM measurements tend to agree better with the predicted PMs (Pawlowski & Kroupa 2013).

The observed distribution of stellar light (and thus stellar mass) in the newly discovered objects can be used to predict the velocity dispersions of the newly discovered objects. The results depend strongly on which dynamical model (Newtonian dynamics or modified Newtonian dynamics, MOND; Milgrom 1983) or which dark matter halo scaling relation is assumed (McGaugh et al. 2007; Walker et al. 2009). We will provide predictions for all these different cases.

This paper is structured as follows. In Section 2, we will compare the positions of the new satellite objects with the VPOS defined by the previously known MW satellites before measuring the effect of adding the new objects to the VPOS plane fit. Our predictions for the PMs of the objects are presented in Section 3, and the predicted velocity dispersions in Section 4. We end with concluding remarks in Section 5.

2 THE VPOS

If the VPOS is a real structure, then it makes a prediction for the probable locations of new satellites. Here, we compare the positions of the new satellite objects with the VPOS as defined by the previously known MW satellite galaxies (Section 2.1). We then determine how the VPOS orientation changes when the new objects are included in the plane fit.

For Kim 1, Lae II, Hor II, Hyd II, Tri II and Peg III, we will use the positions and distances reported in their respective discovery papers, as listed in Table 1. For those satellite objects discovered by both B15 and Koposov et al. (2015a), we will use the average of the two distances estimates. The one exception is the star cluster Kim 2, for which more reliable observational data was obtained in the discovery paper by Kim et al. 2015a, such that we use their distance measurement. We found that our results are statistically robust against either using the B15 or the Koposov et al. (2015a) distances.

Table 1. Compilation of observed properties of the newly detected MW satellite objects.

Object	Suggested names	Type	α (°)	δ (°)	m–M (mag)	$r_\odot$ (kpc)	M_V (mag)	$r_{1/2}$ (arcmin)	$r_{1/2}$ (pc)	Ref.
Kim 1	Kim 1	CC	332.92	7.03	16.5 ± 0.1	19.8 ± 0.9	0.3 ± 0.5	1.2 ± 0.1	6.9 ± 0.6	(1)
Ret II	DES J0335.6-5403	U	53.92	−54.05	17.5	32	-3.6 ± 0.1	$3.8^{+1.0}_{-0.6}$	35^{+9}_{-5}	(2)
	Reticulum 2		53.93	−54.05	17.4	30	-2.7 ± 0.1	3.7 ± 0.2	32 ± 1	(3)
Lae II	Triangulum II	U	33.32	36.18	17.4 ± 0.1	30	-1.8 ± 0.5	$3.9^{+1.1}_{-0.9}$	34^{+9}_{-8}	(4)
Tuc II	DES J2251.2-5836	UD	343.06	−58.57	18.8	58	-3.9 ± 0.2	7.2 ± 1.8	120 ± 30	(2)
	Tucana 2		342.97	−58.57	19.2	69	-4.4 ± 0.1	9.9 ± 1.4	199 ± 28	(3)
Hor II	Horologium II	U	49.13	−54.14	19.5	78	$-2.6^{+0.2}_{-0.3}$	$2.09^{+0.44}_{-0.41}$	47 ± 10	(5)
Hor I	DES J0255.4-5406	U	43.87	−54.11	19.7	87	-3.5 ± 0.3	$2.4^{+3.0}_{-1.2}$	60^{+76}_{-30}	(2)
	Horologium 1		43.88	−54.12	19.5	79	-3.4 ± 0.1	1.3 ± 0.2	30 ± 3	(3)
Phe II	DES J2339.9-5424	U	354.99	−54.41	19.9	95	-3.7 ± 0.4	1.20 ± 0.6	33^{+20}_{-11}	(2)
	Phoenix 2		355.00	−54.41	19.6	83	-2.8 ± 0.2	1.1 ± 0.2	27 ± 5	(3)
Eri III	DES J0222.7-5217	U	35.69	−52.28	19.9	95	-2.4 ± 0.6	$0.4^{+0.3}_{-0.2}$	11^{+8}_{-5}	(2)
	Eridanus 3		35.69	−52.28	19.7	87	-2.0 ± 0.3	0.7 ± 0.3	18 ± 8	(3)
Kim 2	Kim 2	CC	317.21	−51.16	20.1 ± 0.1	104.7 ± 4.1	-1.5 ± 0.5	0.42 ± 0.02	12.8 ± 0.6	(6)
	DES J2108.8-5109		317.20	−51.16	19.2	69	-2.2 ± 0.5	0.6 ± 0.1	12 ± 2	(2)
	Indus 1		317.20	−51.17	20.0	100	-3.5 ± 0.2	1.4 ± 0.4	39 ± 11	(3)
Gru I	Grus 1	U	344.18	−50.16	20.4	120	-3.4 ± 0.3	2.0 ± 0.7	70 ± 23	(3)
Pic I	DES J0443.8-5017	U	70.95	−50.28	20.5	126	-3.7 ± 0.4	$1.2^{+4.2}_{-0.6}$	43^{+153}_{-21}	(2)
	Pictoris 1		70.95	−50.28	20.3	114	-3.1 ± 0.3	0.9 ± 0.2	31 ± 7	(3)
Hyd II	Hydra II	UD	185.44	−31.98	20.64 ± 0.16	134 ± 10	-4.8 ± 0.3	$1.7^{+0.3}_{-0.2}$	68 ± 11	(7)
Peg III	Pegasus III	UD	336.10	5.41	21.56 ± 0.20	205 ± 20	-4.1 ± 0.5	1.85 ± 0.10	110 ± 6	(8)
Eri II	DES J0344.3-4331	UD	56.09	−43.53	22.6	330	-7.4 ± 0.1	1.6 ± 0.6	155 ± 54	(2)
	Eridanus 2		56.09	−43.53	22.9	380	-6.6 ± 0.1	1.6 ± 0.1	172 ± 12	(3)

Notes. Properties of the newly discovered MW satellite objects collected from the literature, the reference from which the data of a given row have been collected is indicated in the last column (labelled 'Ref.'). Type can be CC for confirmed star cluster, UD for unconfirmed dwarf galaxy candidate and U for unclassified (unconfirmed star cluster or ultrafaint dwarf galaxy candidate). The other parameters are α and δ for right ascension and declination of the object, m–M for its distance modulus, $r_\odot$ for the heliocentric distance in kpc, M_V for the absolute V-band magnitude and $r_{1/2}$ for the two-dimensional half-light radius in both arc minutes and parsec. B15 find Ret II and Eri II to have a significant ellipticity ϵ and report their half-light radii as measured along the semimajor axis. We report and use the circularized $r_{1/2}$, which is obtained by multiplying the semimajor axis ellipticity with $\sqrt{1-\epsilon}$. Uncertainties are given if they are specified in the original publication.
Reference: (1) Kim & Jerjen (2015a), (2) B15, (3) Koposov et al. (2015a), (4) Laevens et al. (2015), (5) Kim & Jerjen (2015b); (6) Kim et al. (2015a), (7) Martin et al. (2015), (8) Kim et al. (2015b).

2.1 Comparison to the known VPOS

As a first step, we have compared the positions of the new MW satellite objects with the VPOS plane orientation given by (i) the 27 previously known MW satellite galaxies (hereafter VPOSall) and (ii) the fit to 24 of those galaxies, excluding the three outliers Hercules, Ursa Major and Leo I (hereafter VPOS-3). The respective plane parameters from Pawlowski, Kroupa & Jerjen 2013 are reproduced in the second and third columns of Table 2. As already mentioned by Kim & Jerjen (2015a), Kim et al. (2015a), B15, Martin et al. (2015) and Kim et al. (2015b), the new objects lie close to the VPOS. Table 3 lists their offsets from the VPOSall and VPOS-3. The average offset of the 13 new objects from the VPOSall plane is only 31 kpc, the median is 21 kpc.

Eight objects are particularly close to the best-fitting planes. The seven satellite objects Kim 1, Ret II, Hor I, Hor II, Eri III, Pic I and Peg III have offsets of $\lesssim$20 kpc from the VPOSall, and all but Eri II have offsets of only 11 kpc or less from the VPOS-3. Considering Eri II's large distance of 350 ± 30 kpc from the MW, it is worth noticing that the two distance ratios $d_{\rm VPOSall}/d_{\rm MW}$ and $d_{\rm VPOS\text{-}3}/d_{\rm MW}$ of less than 14 per cent are remarkably small.

The largest offsets are found for the candidate objects Gru I, Hyd II and the star cluster Kim 2. Koposov et al. (2015a) note that Gru I is located close to a CCD chip gap in the DES survey, such that its parameters are more uncertain than those of the other candidates. A smaller distance from the MW would reduce the offset. Furthermore, in particular the two dwarf galaxy candidates Gru I and Hyd II both have large Galactocentric distances, such that despite their relatively large perpendicular offset from the planes their position vectors are only about 30° inclined relative to the planes. In summary, most of the newly reported satellite galaxies and star clusters are qualitatively consistent with the original VPOS.

2.2 Influence of the DES footprint

The region covered by the DES-Y1A1 search area is close to the Magellanic Clouds, and thus not far from the VPOS plane. It might therefore not be surprising that the satellite objects discovered by this survey are close to the VPOS, as argued by B15. To quantify how much of an alignment is expected due to the survey footprint, and thus to test whether it causes the alignment, we have created 10 000 realizations of isotropic DES object positions. To construct these, the angular positions of the 10 DES objects have been randomly selected from an isotropic distribution around the Galactic centre, while their Galactocentric distances have been preserved. Only positions lying within the region covered by the already observed part of the DES footprint were accepted. Positions outside of this region were randomized again until they were within the survey footprint. This guarantees that each randomized realization contains 10 objects which share the same radial distribution as the observed objects. We have then determined the offsets from the VPOSall plane for each position, and determined the mean and median offsets for each set of 10 randomized DES satellite objects.

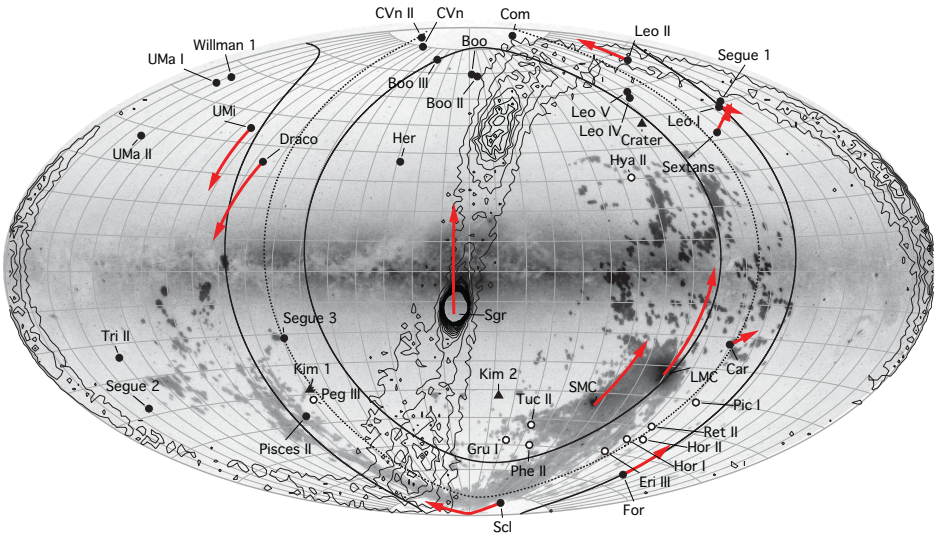

Figure 1. All-sky plot illustrating the positions of the MW satellites relative to the MW (inverted image in the background of the plot). Previously known satellite galaxies are plotted as filled black points, recently discovered satellite objects as white points and star clusters as filled black triangles. The velocities of the 11 classical satellites are indicated by the red arrows, which are the projected 3D velocity vectors determined from the measured line-of-sight velocities and proper motions as compiled in Pawlowski & Kroupa (2013). The dotted line indicates the orientation of the VPOS+new fit. The rms height of the VPOS is illustrated with two solid lines, which show the intersection of the VPOS+new of height 31 kpc with a sphere of 100 kpc radius. The majority of MW satellites fall close to the VPOS, as does the Magellanic Stream (dark patches). Note that the parallax effect due to the offset of the Sun from the Galactic centre (and thus the best-fitting VPOS plane) and the intrinsic thickness of the VPOS increase the scatter of the satellites around the VPOS great circle. The proper motions indicate that eight of the 11 classical satellites are consistent with co-orbiting in the VPOS, while Sculptor is counter-orbiting within the VPOS and Sagittarius is on an orbit perpendicular to both the MW and the VPOS, as also traced by the Sagittarius stream (contour lines indicate particle densities for the simulated stream from Law & Majewski 2010). The background image is by Nidever et al. (2010), NRAO/AUI/NSF and Meilinger, Leiden-Argentine-Bonn Survey, Parkes Observatory, Westerbork Observatory, Arecibo Observatory (see http://www.nrao.edu/pr/2010/magstream/).

Table 2. New plane fit parameters (all objects except confirmed star clusters).

Name	VPOSall	VPOS-3	VPOS+new	VPOS+new-4	VPOSsouth	VPOSnorth
$\boldsymbol{n}\begin{pmatrix} l \\ b \end{pmatrix}$ (°)	$\begin{pmatrix} 155.6 \\ -3.3 \end{pmatrix}$	$\begin{pmatrix} 169.5 \\ -2.8 \end{pmatrix}$	$\begin{pmatrix} 164.0 \\ -6.9 \end{pmatrix}$	$\begin{pmatrix} 169.4 \\ -6.1 \end{pmatrix}$	$\begin{pmatrix} 169.3 \\ -7.2 \end{pmatrix}$	$\begin{pmatrix} 157.7 \\ -8.9 \end{pmatrix}$
$D_{\rm MW}$ (kpc)	7.9	10.4	2.5	5.4	3.6	3.0
Δ (kpc)	29.3	19.9	30.9	21.3	22.3	36.4
c/a	0.301	0.209	0.313	0.224	0.356	0.475
b/a	0.576	0.536	0.579	0.566	0.619	0.623
$N_{\rm members}$	27	24	38	34	19	19
Outliers excluded?	No	Yes	No	Yes	No	No
Includes new objects?	No	No	Yes	Yes	Yes	Yes

Notes. Parameters of the plane fits: $\boldsymbol{n}$: the direction of the normal vector (minor axis) of the best-fitting plane in Galactic longitude l and latitude b.
$D_{\rm MW}$: offset of the planes from the centre of the MW.
Δ: rms height from the best-fitting plane of the MW satellite objects included in the fit.
c/a and b/a: short- and intermediate-to-long axial ratios, determined from the rms heights in the directions of the three axes.
$N_{\rm members}$: number of objects used for the fits.

Fig. 2 shows the resulting distribution of the mean and the median offsets of these 10 000 realisations. The 10 observed objects have an average offset of 28 kpc and a median offset of 18 kpc. If they were drawn from an isotropic distribution, the expected (average) mean and median would be considerably (about 50 per cent) larger: 41 and 31 kpc, respectively. Of all randomized realisations, 91 per cent have a larger mean offset, and 96 per cent have a larger median offset than the observed values. This indicates that the observed alignment is indeed stronger than expected from the current survey footprint alone, but the significance of this conclusion is not extremely high. This might change once the full DES footprint is covered, in particular if at larger distances from the VPOS fewer satellites are discovered.

2.3 Effects on the best-fitting VPOS

We now update the plane fits by including the new objects. Since we use the same fitting routine and adopt the same parameters as in Pawlowski et al. (2013), we refer the reader to that paper for further information on the method.

To be consistent with the previous plane fitting analysis that focused on satellite galaxies, in the following, we add only those 11 new objects to the plane fit sample which are likely but still unconfirmed satellite galaxies. The two objects Kim 1 and 2, which have already been identified as star clusters through follow-up observations are not included. We also exclude Eri II from the fit because its large distance estimate places it outside of the virial radius of the

Table 3. Galactocentric distances, Cartesian positions and offsets of MW satellites from the VPOS plane fits (in kpc).

Name	$d_{\rm MW}$	x	y	z	$d_{\rm VPOSall}$	$d_{\rm VPOS-3}$	$d_{\rm VPOS+new}$	$d_{\rm VPOS+new-4}$	$d_{\rm VPOSsouth}$	$d_{\rm VPOSnorth}$
The Galaxy	0.0	0.0	0.0	0.0	8	10	3	5	4	3
Canis Major	13.4	− 11.9	− 6.2	− 1.0	**1**	**1**	**7**	**5**	**7**	11
Sagittarius dSph	18.4	17.1	2.5	− 6.4	**23**	**28**	**19**	**22**	**21**	12
Segue (I)	27.9	− 19.4	− 9.5	17.7	**5**	**7**	**12**	**11**	12	**15**
Ursa Major II	38.0	− 30.6	11.6	19.2	**26**	**23**	**30**	**27**	29	**35**
Bootes II	39.5	6.6	− 1.7	38.9	**17**	**19**	**14**	**17**	14	**10**
Segue II	40.8	− 31.8	13.9	− 21.4	**29**	**26**	**35**	**32**	**33**	41
Willman 1	42.9	− 27.7	7.6	31.8	**22**	**20**	**25**	**22**	25	**29**
Coma Berenices	44.9	− 10.6	− 4.3	43.4	**3**	**3**	**1**	**1**	2	**4**
Bootes III	45.8	1.3	6.9	45.3	**9**	**13**	**7**	**11**	8	**2**
LMC	50.0	− 0.6	− 41.8	− 27.5	**24**	**16**	**11**	**10**	**9**	10
SMC	61.2	16.5	− 38.5	− 44.7	**38**	**33**	**25**	**25**	**24**	23
Bootes (I)	64.0	14.8	− 0.8	62.2	**26**	**29**	**25**	**27**	25	**20**
Draco	75.9	− 4.4	62.2	43.2	**21**	**4**	**15**	**6**	9	**27**
Ursa Minor	77.8	− 22.2	52.0	53.5	**33**	**19**	**28**	**21**	24	**38**
Sculptor	86.0	− 5.2	− 9.8	− 85.3	**2**	**3**	**10**	**7**	**8**	16
Sextans (I)	89.0	− 36.7	− 56.9	57.8	**2**	**13**	**9**	**14**	16	**5**
Ursa Major (I)	101.6	− 61.1	19.8	78.7	**53**	51	**54**	51	54	**57**
Carina	106.8	− 25.1	− 95.9	− 39.8	**25**	**1**	**2**	**6**	**6**	9
Hercules	126.1	84.1	50.7	79.1	**71**	94	**83**	93	89	**68**
Fornax	149.3	− 41.3	− 51.0	− 134.1	**17**	**30**	**40**	**42**	**41**	40
Leo IV	154.8	− 15.1	− 84.8	128.6	**39**	**18**	**29**	**21**	18	**37**
Canes Venatici II	160.6	− 16.5	18.6	158.7	**6**	**2**	**1**	**3**	5	**4**
Leo V	178.6	− 21.5	− 91.9	151.7	**37**	**14**	**28**	**18**	16	**38**
Pisces II	181.1	14.9	121.7	− 133.3	**38**	**4**	**34**	**17**	**19**	57
Canes Venatici (I)	217.5	2.1	37.0	214.3	**6**	**17**	**20**	**24**	19	**14**
Leo II	235.9	− 77.3	− 58.3	215.2	**26**	**46**	**30**	**38**	42	**20**
Leo I	257.4	− 123.6	− 119.3	191.7	**45**	83	**60**	76	79	**41**
Kim I	19.1	− 2.7	14.4	− 12.3	2	4	6	1	3	13
Ret II	33.0	− 9.7	− 20.4	− 24.1	6	3	**4**	**3**	**4**	7
Lae 2 (Tri II)	36.6	− 29.8	17.4	− 12.2	27	23	**32**	**28**	**30**	39
Tuc II	59.2	24.4	− 20.4	− 49.9	36	35	**26**	**28**	**27**	20
Hor II	80.0	− 9.6	− 48.7	− 62.7	16	7	**1**	**1**	**2**	4
Hor I	83.5	− 7.2	− 48.0	− 67.9	18	9	**2**	**0**	**1**	3
Phe II	88.1	28.7	− 27.2	− 78.8	41	40	**28**	**30**	**29**	23
Eri III	91.2	− 4.3	− 46.0	− 78.7	19	11	**3**	**1**	**1**	4
Kim II (Ind I)	98.9	67.5	− 17.3	− 70.2	72	76	63	67	66	55
Grus 1	116.4	50.6	− 23.0	− 102.2	57	59	**45**	**48**	**48**	38
Pic I	121.9	− 28.1	− 88.2	− 79.2	15	5	**8**	**14**	**14**	6
Hydra II	129.0	40.8	− 102.4	66.8	92	72	**79**	71	70	**85**
Pegasus III	203.1	44.3	143.5	− 136.8	21	21	**13**	**8**	**6**	40
Eri II	365.0	− 86.2	− 211.4	− 284.7	4	50	51	69	66	35

Notes. MW satellite distances from the MW ($d_{\rm MW}$), Galactocentric Cartesian x, y and z positions and offsets from the different best-fitting VPOS planes: all 27 satellite galaxies considered in Pawlowski et al. (2013, VPOSall), the same sample but excluding three outliers (VPOS-3) and the fit to the 27 known and confirmed MW satellite galaxies plus all new objects except those which have been identified as star clusters (VPOS+new, i.e. the VPOSall sample plus Ret II, Lae 2, Tuc II, Hor I and II, Phe II, Eri III, Gru I, Pic I, Hyd II and Peg III). For those of the new objects discovered by both B15 and K15, we assume that their heliocentric distances are the average of the two distance estimates when fitting the plane. If an object was included in the plane fit its respective offset if printed in boldface.

MW (≈250 kpc), it thus should not be considered a satellite galaxy of the MW.

For the full VPOS sample (called VPOS+new in Table 2), we use all 27 previously identified satellites plus the 11 new satellite objects. Our analysis shows that even though the sample size used for the fit has increased by 40 per cent, and the number of objects in the Southern Galactic hemisphere doubled, the VPOS parameters remain essentially unchanged. The direction of the plane normal $\boldsymbol{n}$ changes by only about 9°, to larger Galactic longitude and slightly lower Galactic latitude. This normal is closely aligned (within 9°) with the normal direction of the 'classical' disc of satellites defined by the 11 brightest MW satellites, which points to $(l, b) = (157.^{\circ}3, -12.^{\circ}7)$. Because these are the brightest MW satellites, their distribution should be the least affected by biases due to uneven sky coverages, but low-number statistics are a concern.

Our plane fit routine does not require the fitted plane to pass through the MW centre. This extra freedom acts as a consistency check for whether a found plane can be dynamically stable.[1] It is therefore arguably the most interesting finding that the new offset from the MW centre $D_{\rm MW}$, is reduced from 7.9 to only 2.5 kpc. This might indicate that it needed more satellites in the Southern

[1] If a satellite plane has a large offset from its host's centre (such as Plane 2 in Shaya & Tully 2013), the satellites cannot orbit within the plane and the arrangement must be a transient feature.

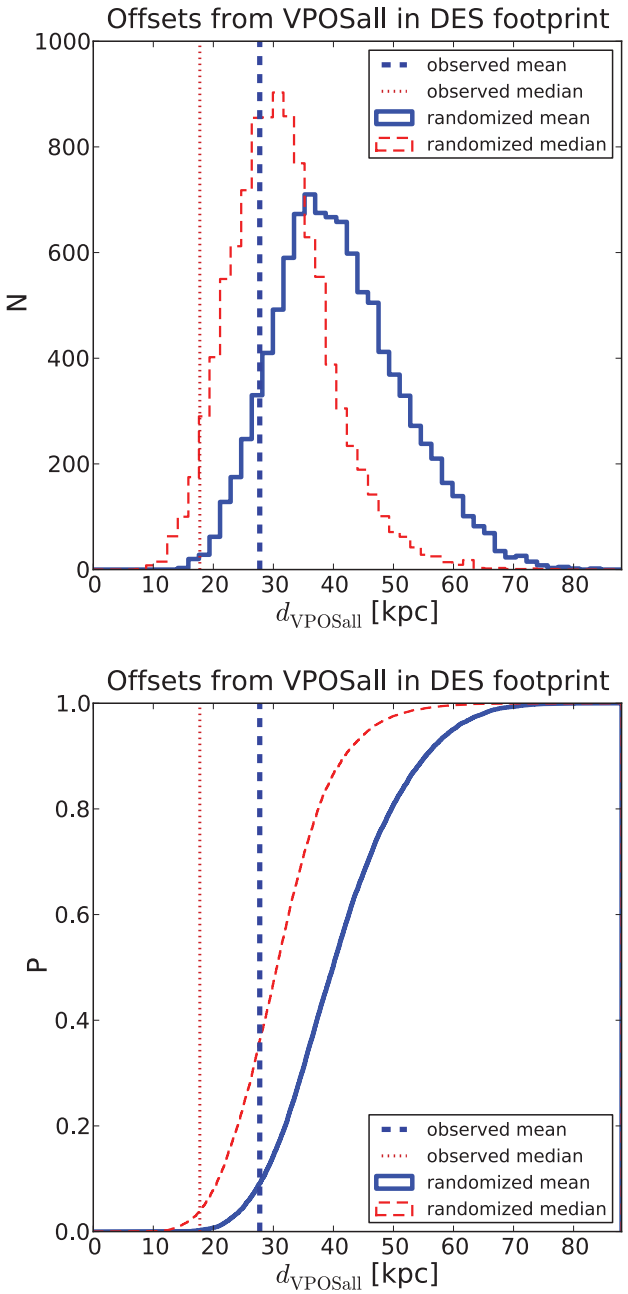

Figure 2. Histogram (upper panel) and cumulative distribution (lower panel) of mean and median offsets for 10 000 randomized distributions of the 10 stellar systems within the DES-Y1A1 footprint, as discussed in Section 2.2. Even though the DES footprint is close to the VPOS, the observed mean and median (thick solid blue and thinner dashed red histograms, respectively) offsets of the 10 objects (vertical dashed and dotted lines, respectively) are smaller than expected for isotropically distributed objects.

Galactic hemisphere to 'balance' the VPOS out in the MW centre. Despite the overall shift to smaller MW offsets, both measures of the plane thickness, the root-mean-square (rms) height Δ and the short-to-long axial ratio c/a, remain almost unchanged (they both increase by a few per cent) if the additional satellite galaxy candidates are included in the fit. The resulting values $\Delta = 30.9$ kpc and $c/a = 0.313$ are both at least 50 per cent smaller than those expected for the same number of satellites objects drawn from isotropic distributions or from sub-halo distributions in cosmological simulations of MW equivalents (see e.g. fig. 3 of Pawlowski & McGaugh 2014b).

The distances of the satellites from this new best-fitting plane are also compiled in Table 3. Not surprisingly, the new objects have smaller offsets from the VPOS plane if they are included in the plane fit. Since the plane orientation has not changed dramatically compared to the VPOSall, the same objects tend to be closest to the new fit, too.

In addition to fitting a plane to all 27 known plus the 11 new satellite candidates, we have also constructed a sample analogous to the VPOS-3 by excluding the four outliers with offsets of more than 50 kpc from the VPOS+new fit. These are the three previously identified outliers Hercules, Ursa Major I and Leo I, as well as the newly discovered object Hyd II. We note that Leo I has a PM indicating that it does not orbit within the VPOS. It might not even be a true MW satellite given its large Galactocentric distance and high velocity. This VPOS+new-4 has a very similar orientation as the VPOS+new (inclined by about 6°) but is significantly thinner ($\Delta = 21.3$ kpc, $c/a = 0.224$). It is almost identical in orientation and thickness to the VPOS-3, but also has a smaller offset from the MW centre.

As reported before (Pawlowski et al. 2013), the VPOS plane is oriented almost exactly like the current orbital plane of the LMC, which has an orbital pole (direction of angular momentum) pointing towards $(l, b) = (175.^{\circ}4, -5.^{\circ}7)$ (Pawlowski & Kroupa 2013), less than 12° inclined with respect to the VPOS+new and only 6° with respect to the VPOS+new-4. This supports the almost 40 yr old notion by Kunkel & Demers (1976) and Lynden-Bell (1976) that most MW satellites seem to share the same orbital plane as the Magellanic Clouds.

Fig. 3 shows the distribution of known satellite objects around the MW from both an edge-on and face-on views of the updated VPOS+new. Newly discovered satellite objects are plotted as light blue diamonds if they have been confirmed to be star clusters, or as bright-green stars. It is obvious that most of the recently discovered satellite galaxy candidates lie within the VPOS plane at intermediate distances from the MW. The majority populate a region where previously known classical MW satellites (yellow dots in the figure) are situated.[2] This is illustrated by the face-on VPOS+new view in the lower panel of Fig. 3, in which the majority of new discoveries populate the lower (southern) left quadrant of the VPOS plane.

This panel also illustrates how isolated the new MW satellite Pegasus III is. As pointed out by Kim et al. (2015b), its only known close neighbour at a distance of about 37 kpc is Pisces II. The next-closest known MW satellites are found at distances of 170 kpc or more. The whole lower (southern) right quadrant of the VPOS in the lower panel of Fig. 3 appears to be surprisingly devoid of known MW satellites. None of the 11 classical MW satellites falls into this region at Galactocentric distances beyond about 30 kpc (the closest one, Sagittarius, lies at the edge of this quadrant but is known to orbit perpendicular to the VPOS). Interestingly, part of this quadrant was surveyed by the Sloan Extension for Galactic Understanding and Exploration (SEGUE) extension of the SDSS survey, within which Pisces II, the only previously known faint MW satellite galaxies in this region, was found. The next-closest known structure, also found in the data of the SDSS survey, is the Pisces overdensity (Watkins et al. 2009) at a distance of 130 kpc from Pegasus III (green triangle

[2] The LMC and Small Magellanic Cloud (SMC), Carina, Fornax and Sculptor.

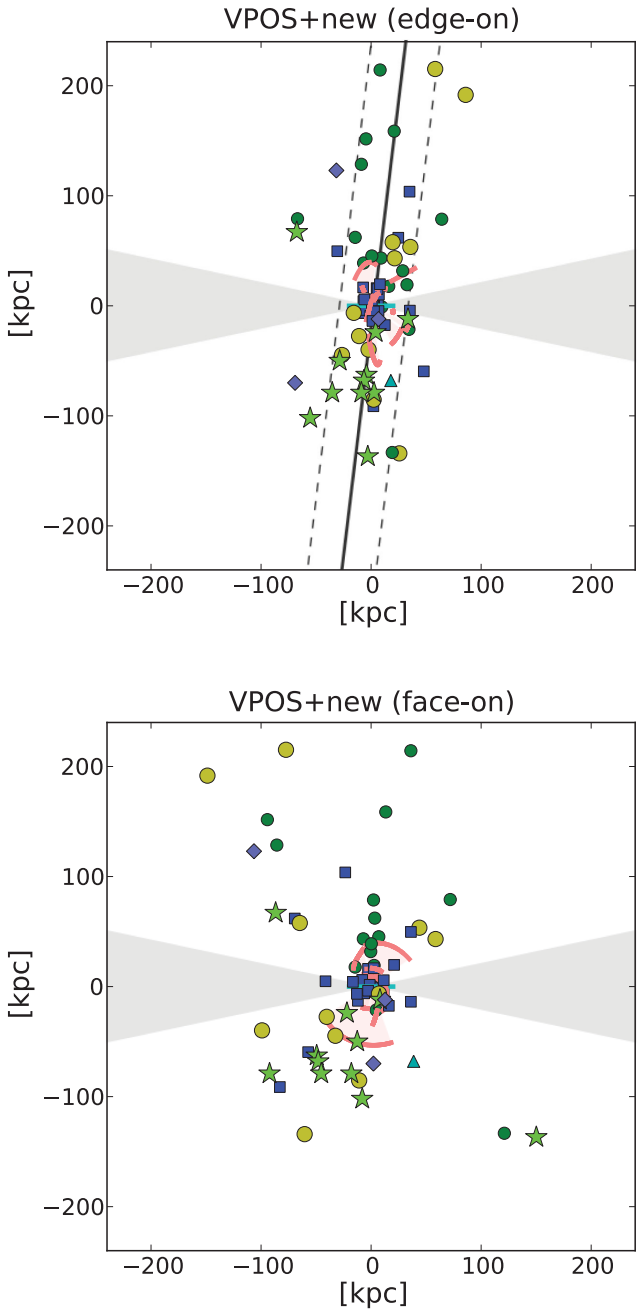

Figure 3. Distribution of satellite objects in Cartesian coordinates around the MW. The upper panel shows the VPOS+new fit edge-on (black solid line, the dashed lines indicate the rms height), the lower panel shows a view rotated by 90°, in which the VPOS is oriented approximately face-on. In this view, the MW satellites with measured proper motions preferentially orbit in the clockwise direction. The 11 brightest (classical) MW satellite galaxies are plotted as yellow dots, the fainter satellite galaxies as smaller green dots and globular clusters classified as young halo objects as blue squares. New objects confirmed to be star clusters (PSO J174.0675-10.8774/Crater in the north, Kim 1 and 2 in the south) are plotted as lighter blue diamonds, all other new objects as bright-green stars. The red lines in the centre indicate the position and orientation of streams in the MW halo. They preferentially align with the VPOS, but are mostly confined to the innermost regions of the satellite distribution. Both plots are centred on the MW (cyan line) which is seen edge-on. The grey wedges indicate the region (±12°) around the MW disc, where satellite galaxies might be obscured by the Galaxy.

in Fig. 3). The overdensity might be the remnant of a dwarf galaxy or star cluster currently being disrupted, and is also aligned with the Magellanic Stream and the VPOS.

2.4 Dividing the VPOS: north–south differences?

For a long time, the majority of known MW satellites galaxies lay in the Galactic north because the SDSS initially concentrated on that part of the sky. With the discovery of new satellite galaxy candidates, the numbers of southern objects approach that of the northern ones (19 each, if all of the new candidate objects turn out to be bona-fide satellite galaxies). The comparable sample size allows us to fit the VPOS for the southern and northern satellite populations separately. Such a split might reveal whether the VPOS is systematically tilted or bent, for example due to precession of the satellites on their orbits or because of non-symmetric infall of the VPOS-satellites. Due to the Galactic disc which possibly obscures satellites along the Galactic equator, splitting the satellites into a northern and southern sample is the most sensible separation.

The resulting plane fit parameters for the two sub-samples are similar to each other and to the VPOS+new plane fitted to all objects (see Table 2). Both the northern and the southern VPOS plane fits are inclined by only 6° relative to the total VPOS+new plane fit. They both are almost polar (the normal vectors have Galactic latitudes of $b = -7°$ and $-9°$, for the southern and the northern satellites, respectively), have a very similar orientation (inclined by less than 12°), have essentially the same small offset from the Galactic centre ($D_{\rm MW} \approx 3$ kpc) and are similarly thin ($\Delta_{\rm rms} = 22$ versus 36 kpc). However, while the thinner, southern plane shares its orientation with the orbital plane of the Large Magellanic Cloud (LMC) (and the VPOS-3 plane fits) to within 6°, the northern one is more inclined (18°).

Interestingly, the orientation and thickness of the northern plane is strongly affected by the four outliers, which are all northern objects. If they are excluded from the northern VPOS fit, the resulting plane parameters are extremely similar to those of the southern fit: the normal to the best-fitting plane points to $(l, b) = (168.^{\circ}5, -3.^{\circ}3)$, the rms height of the plane is $\Delta_{\rm rms} = 20$ kpc, but the offset from the MW centre is $D_{\rm MW} = 11$ kpc. Even without excluding the outliers from the northern satellite sample, the plane parameters of the northern (VPOSnorth) and the southern (VPOSsouth) fits agree well. We therefore conclude that the current data suggest that the northern and the southern parts of the VPOS have similar properties and orientations. This might also indicate that observational biases – which are different for the Northern and Southern hemispheres – do not affect the determined plane orientations significantly.

2.5 The distant object Eri II

The two current distance estimates for Eri II are 330 (B15) or 380 kpc (Koposov et al. 2015a). These place the object barely outside of the virial radius expected for the MW (about 250–300 kpc). If its position just beyond the MW halo is confirmed, this would make Eri II the closest known non-satellite dwarf galaxy in the Local Group (LG), closer than the neighbours Phoenix and Leo T at about 420 kpc distance.

Eri II aligns well with the VPOS plane, even though it was excluded from the fit due to its large distance. In this regard, it might be interesting to check where Eri II lies with respect to the dominating plane of non-satellite galaxies in the LG, termed LG plane 1 (LGP1; Pawlowski et al. 2013; Pawlowski & McGaugh 2014a). LGP1 consists of about 10 LG dwarf galaxies which have distances

of more than 300 kpc from both the MW and M31. It is an extremely narrow plane, with rms height of about 50 kpc and a maximum diameter of 2 Mpc, which stretches from M31 to the MW and beyond. Approximately in Eri II's direction LGP1 has its closest approach to the MW, of about 180 kpc. Depending on its exact position, Eri II has an offset of about 100 kpc from LGP1. It therefore may potentially be a member of this structure. Assuming Eri II to be part of and perfectly aligned with LGP1, we would have predicted it to be closer than the current estimates by about 50–100 kpc. Measuring Eri II's line-of-sight velocity might shed more light on whether an association with LGP1 is likely. All LGP1 dwarf galaxies have line-of-sight velocities relative to the local standard of rest which follow the Magellanic Stream velocity at their positions (see Fig. 6). If Eri II follows the same trend, its velocity should be in the range of 50–250 km s^{-1}.

The spatial position of Eri II thus places it at the intersection of LGP1 and the VPOS, a very interesting position holding the promise that Eri II might provide important clues on if and how the VPOS is connected to the larger scale structure of dwarf galaxies in the LG.

3 PREDICTED PROPER MOTIONS

Out of the 11 MW satellite galaxies for which PMs have been measured, eight are consistent with co-orbiting in the same sense within the VPOS, while Sculptor also orbits within the VPOS but in the opposite direction (Metz, Kroupa & Libeskind 2008; Pawlowski & Kroupa 2013). This orbital alignment finds further support in the alignment of several streams in the MW halo with the VPOS (Pawlowski et al. 2012), most prominently the Magellanic Stream. That satellite galaxy planes appear to be rotating structures is also supported by the M31 satellite plane which shows coherent line-of-sight velocities indicative of rotation (Ibata et al. 2013). In addition, the unexpected anti-correlation of velocities for diametrically opposite satellite galaxy pairs in the SDSS indicates that co-orbiting satellite galaxy planes might be ubiquitous (Ibata et al. 2014).

Since most of the newly discovered objects are closely aligned with the VPOS-3 plane and thus with the average orbital plane of the co-orbiting MW satellite galaxies, we can empirically predict the PM of the new MW satellite objects by using the method presented in Pawlowski & Kroupa (2013). This method assumes that the object it either co- or counter-orbiting in the plane defined by the current satellite positions. Because no line-of-sight velocity has yet been measured for most of the new objects, we assume that they have minimum (i.e. zero) Galactocentric line-of-sight velocities min $(v_{\rm los})$, calculated as the negative of the component of the Galactocentric Solar motion in the direction of the object. The exact line-of-sight velocity of an object does not affect the orientation of the predicted PM, but only constrains the maximum and minimum predicted PM to values such that it remains bound to the MW. By assuming a minimum Galactocentric line-of-sight velocity, the predicted PM range will be maximal. Once line-of-sight velocities have been measured they can be used to put tighter constraints on the expected range in PMs.

To make the prediction compatible with those presented in Pawlowski & Kroupa (2013) and Pawlowski & Kroupa (2014), we adopt the same values for the circular velocity of the MW, the solar motion with respect to the local standard of rest and the Galactocentric distance of the Sun. This is also one reason why the orientation of the VPOS-3 was used in this prediction instead of the new fit. Another reason is that it is not yet known with certainty which of the new objects are satellite galaxies and which are star clusters that should not be part of the VPOS fit. However, since the measured VPOS orientation changes only minimally if the new objects are included in the plane fits, this choice does not strongly affect the predicted PMs anyway. We again use the average of the distances reported by K15 and B15 for those objects discovered by both, except for Kim 2 for which we use the more reliable measurement from Kim et al. (2015a) based on follow-up observations. We also use the method to predict Eri II's PM, but caution that its large distance from the MW makes it unlikely that it is a satellite gravitationally bound to the MW.

The resulting PM predictions are compiled in Table 4 and illustrated in Fig. 4. The table also provides the angle between the Galactocentric position of the object and the VPOS-3 plane, $\theta^{\rm predicted}_{\rm VPOS-3}$, which is equal to the minimum possible inclination between the orbit of the object and the VPOS-3 plane. These angles tend to be small, again illustrating that most of the new objects are closely aligned with the satellite plane.

If future PM measurements reveal that more MW satellites follow the strong velocity alignment of the classical MW satellites with the VPOS, this would dramatically increase the significance of their alignment. While the probability of a position drawn from an isotropic distribution to be within an angle θ from a given plane is $P_{\rm vector} = \sin(\theta)$, the probability that a randomly oriented orbital plane is aligned to within θ with a given plane is only $P_{\rm plane} = 1 - \cos(\theta)$. For example, while 71 per cent of isotropically distributed positions are expected to lie within 45° of a randomly oriented plane, only 29 per cent of isotropically distributed orbital poles are expected to be within 45° of the plane's normal vector.

3.1 Interpreting PM predictions

We caution against interpreting the PM predictions too tightly. The predicted PM ranges are derived from assuming the best possible alignment of the orbital pole with the normal to a satellite plane. Because the VPOS has a finite rms height, the orbits of most satellites cannot be perfectly aligned. The orbital poles of the MW satellites therefore have a minimum intrinsic scatter around their average direction. In addition, all satellites which have orbital planes inclined from the VPOS will at some point during their orbits be perfectly aligned with the VPOS. If observed at that position we would predict the satellites to orbit perfectly within the VPOS, even though they do not.

The width of the VPOS can give us an idea of this intrinsic scatter in orbital pole directions (to which scatter due to PM measurement uncertainties will be added). The VPOS-3 which is used for the PM prediction has an rms axial ratio of $c/a = 0.2$. This gives an approximate opening angle[3] of $2 \times \arcsin(0.2) \approx 23°$. This estimate agrees with the measured spherical standard deviation of the eight best-aligned orbital poles derived from the observed PMs, which is about 27°. To meaningfully compare the predicted and observed PMs therefore requires that we measure the angle between the orbital poles (or the measured orbital pole and the VPOS normal vector assumed for the prediction). If the inclination is less than the expected scatter, the measurement can be said to agree with the prediction.

[3] Strictly speaking the angle depends on (and decreases with) the radial distance from the MW, because the VPOS is a plane-like structure.

Table 4. Predicted PMs of MW satellite objects assuming they orbit within the VPOS-3.

Name	l (°)	b (°)	$r_\odot$ (kpc)	min ($v_{\rm los}$) (km s^{-1})	$\theta^{\rm predicted}_{\rm VPOS-3}$ (°)	$[v_{\rm min}, v_{\rm max}]$ (km s^{-1})	$\begin{pmatrix}\mu_\alpha \cos\delta \\ \mu_\delta\end{pmatrix}_{\rm co}$ (mas yr^{-1})	$\begin{pmatrix}\mu_\alpha \cos\delta \\ \mu_\delta\end{pmatrix}_{\rm counter}$ (mas yr^{-1})
Kim 1	68.5	−38.4	20	−182	17.8	[50, 595]	$\begin{pmatrix}[+0.92,\ +4.55] \\ [-2.17,\ -6.72]\end{pmatrix}$	$\begin{pmatrix}[+0.26,\ -3.36] \\ [-1.34,\ +3.21]\end{pmatrix}$
Ret II	266.3	−49.7	32	168	11.9	[50, 518]	$\begin{pmatrix}[+1.43,\ +4.41] \\ [-0.66,\ -1.61]\end{pmatrix}$	$\begin{pmatrix}[+0.80,\ -2.18] \\ [-0.46,\ +0.48]\end{pmatrix}$
Tuc II	328.1	−52.3	63	81	25.3	[50, 455]	$\begin{pmatrix}[+0.33,\ +0.74] \\ [-0.90,\ -2.20]\end{pmatrix}$	$\begin{pmatrix}[+0.23,\ -0.18] \\ [-0.59,\ +0.71]\end{pmatrix}$
Hor II	268.5	−52.2	79	160	2.4	[50, 429]	$\begin{pmatrix}[+0.57,\ +1.50] \\ [-0.31,\ -0.68]\end{pmatrix}$	$\begin{pmatrix}[+0.32,\ -0.61] \\ [-0.21,\ +0.17]\end{pmatrix}$
Hor I	271.4	−54.7	83	151	1.0	[50, 421]	$\begin{pmatrix}[+0.54,\ +1.39] \\ [-0.33,\ -0.74]\end{pmatrix}$	$\begin{pmatrix}[+0.32,\ -0.53] \\ [-0.22,\ +0.19]\end{pmatrix}$
Phe II	323.7	−59.7	89	77	19.5	[50, 423]	$\begin{pmatrix}[+0.31,\ +0.73] \\ [-0.59,\ -1.35]\end{pmatrix}$	$\begin{pmatrix}[+0.20,\ -0.21] \\ [-0.39,\ +0.37]\end{pmatrix}$
Eri III	275.0	−59.6	91	132	0.3	[50, 409]	$\begin{pmatrix}[+0.49,\ +1.19] \\ [-0.37,\ -0.81]\end{pmatrix}$	$\begin{pmatrix}[+0.29,\ -0.41] \\ [-0.24,\ +0.20]\end{pmatrix}$
Kim 2	347.2	−42.1	105	38	41.9	[50, 390]	$\begin{pmatrix}[+0.03,\ +0.08] \\ [-0.60,\ -1.28]\end{pmatrix}$	$\begin{pmatrix}[+0.01,\ -0.04] \\ [-0.40,\ +0.29]\end{pmatrix}$
Gru I	338.7	−58.2	120	49	24.9	[50, 369]	$\begin{pmatrix}[+0.19,\ +0.41] \\ [-0.49,\ -1.00]\end{pmatrix}$	$\begin{pmatrix}[+0.12,\ -0.10] \\ [-0.32,\ +0.19]\end{pmatrix}$
Hyd II	295.6	30.5	132	187	28.9	[50, 361]	$\begin{pmatrix}[-0.18,\ +0.03] \\ [-0.09,\ +0.36]\end{pmatrix}$	$\begin{pmatrix}[-0.25,\ -0.46] \\ [-0.24,\ -0.69]\end{pmatrix}$
Pic I	257.4	−41.2	120	191	7.1	[50, 361]	$\begin{pmatrix}[+0.35,\ +0.90] \\ [-0.11,\ -0.16]\end{pmatrix}$	$\begin{pmatrix}[+0.18,\ -0.36] \\ [-0.10,\ -0.05]\end{pmatrix}$
Peg III	69.8	−41.8	205	−174	2.9	[50, 273]	$\begin{pmatrix}[+0.10,\ +0.24] \\ [-0.22,\ -0.40]\end{pmatrix}$	$\begin{pmatrix}[+0.04,\ -0.10] \\ [-0.13,\ +0.05]\end{pmatrix}$
Eri II	249.8	−51.6	363	154	9.3	[50, 105]	$\begin{pmatrix}[+0.12,\ +0.15] \\ [-0.07,\ -0.08]\end{pmatrix}$	$\begin{pmatrix}[+0.07,\ +0.04] \\ [-0.06,\ -0.05]\end{pmatrix}$

Notes. l, b, $r_\odot$: heliocentric position of the MW satellite object in Galactic longitude and latitude and radius.
min ($v_{\rm los}$): heliocentric line-of-sight velocity that minimizes the line-of-sight component of its Galactocentric velocity (i.e. the negative of the Galactocentric solar velocity component in the direction of the object).
$\theta^{\rm predicted}_{\rm VPOS-3}$: the smallest possible inclination between the orbital plane of the satellite galaxy and the VPOS-3 plane, defined by the angle between the Galactocentric position and the plane normal.
$v_{\rm min}$, $v_{\rm max}$: the range of PMs is constrained by adopting this range of minimum and maximum absolute speeds for the objects. The minimum is set to 50 km s^{-1}, the maximum determined by requiring the object to be approximately bound to the MW (see Pawlowski & Kroupa 2013 for details).
$\begin{pmatrix}\mu_\alpha \cos\delta \\ \mu_\delta\end{pmatrix}_{\rm co}$ and $\begin{pmatrix}\mu_\alpha \cos\delta \\ \mu_\delta\end{pmatrix}_{\rm counter}$: predicted PM range if co- or counter-orbiting.

4 PREDICTED VELOCITY DISPERSIONS

Here, we attempt to predict the internal velocity dispersions of the newly discovered satellites from their reported photometric properties. Since it is unclear whether some of these objects are dwarf satellite galaxies or star clusters, we consider both possibilities. We consider both conventional gravity and MOND (Milgrom 1983). Since differences in the photometric properties reported for the objects translate into differences in the predicted velocity dispersions, we make predictions using each of the reported sets of properties. Our results are compiled in Table 5 in the order in which they are listed in Table 1.

4.1 Star clusters

If the newly discovered objects are star clusters, then they may be devoid of dark matter. In this case, their velocity dispersions follow directly from the virial relation and the observed stellar mass and half-light radii:

$$\sigma \approx \left(\frac{GM_*}{3r_{\frac{1}{2}}}\right)^{1/2}, \quad (1)$$

where $r_{\frac{1}{2}}$ is the 3D half-light radius (estimated as 4/3 the effective radius $r_{1/2}$) and $M_* = \Upsilon_* L_V$. To estimate the stellar mass, we assume a mass-to-light ratio of $\Upsilon_* = 2\,{\rm M}_\odot\,{\rm L}_\odot^{-1}$. This is extremely uncertain (see Section 4.4.2). The velocity dispersions predicted in this way are given in Table 5. These are low-luminosity systems, so the predicted velocity dispersions are small: <1 in all cases, and <0.5 km s^{-1} in all but one case. However, the disruption of such dark matter free systems on their orbits around the MW can increase their *apparent* mass-to-light ratios substantially (Kroupa 1997). This successfully predicted an object like the later discovered MW satellite Hercules (see the discussion in Kroupa et al. 2010).

4.2 Scaling relations

If the newly discovered objects are dwarf satellite galaxies, then we expect them to reside within dark matter sub-haloes. If this is the case, the kinematics are presumably dominated by dark matter as with the other known dwarfs. We then anticipate higher velocity dispersions.

There is no universally agreed method to predict the velocity dispersions of individual dwarf satellite galaxies in ΛCDM. The correlation between luminosity and halo mass is exceedingly weak

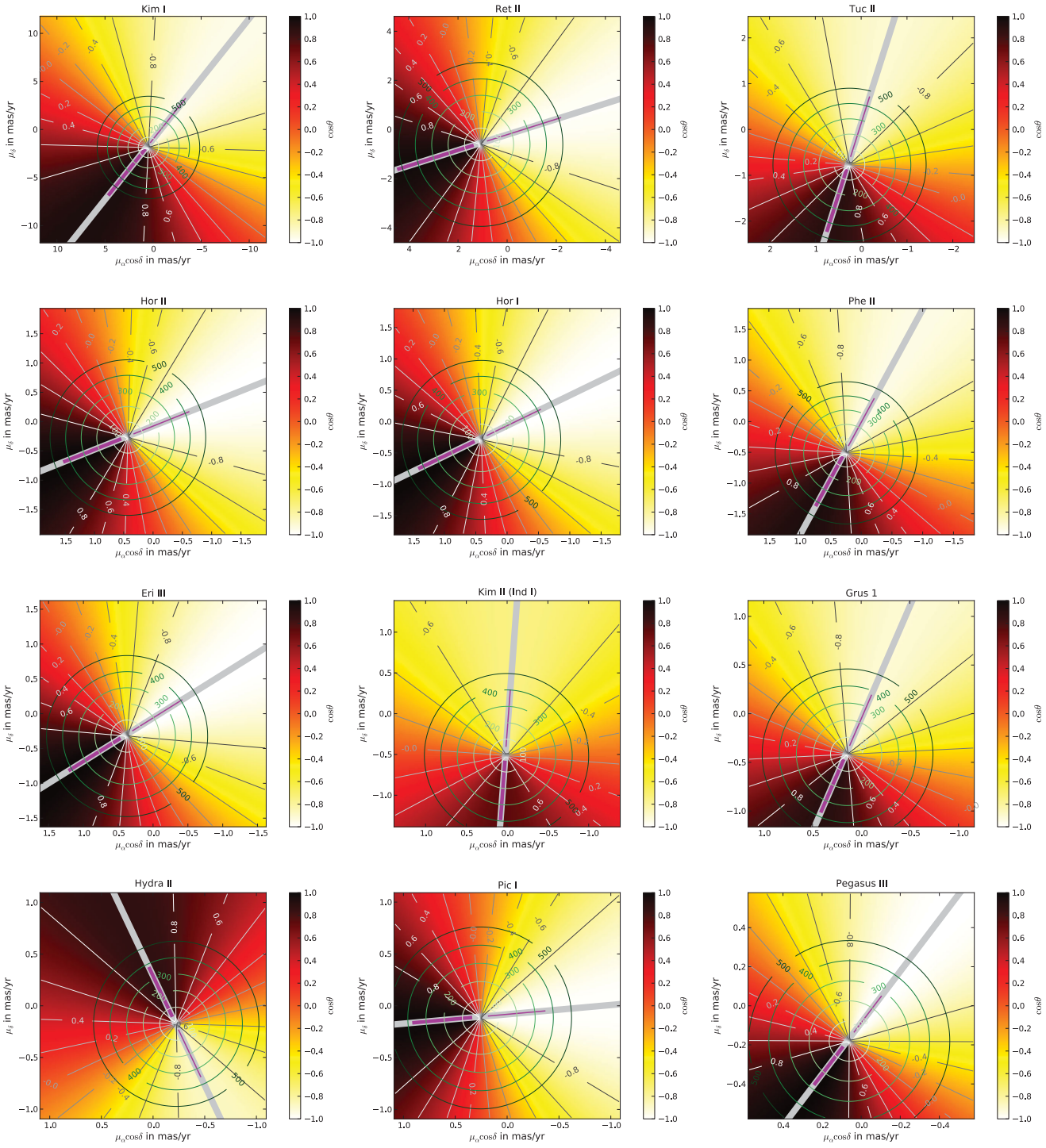

Figure 4. Predicted proper motions of the new MW satellite objects assuming that they move within the VPOS-3 (which is closely aligned with the orbital plane of the LMC). The map illustrates the cosine of the angle θ between the VPOS-3 plane (the plane fitted to all confirmed satellite galaxies except three outliers, see Pawlowski et al. 2013 for more details) and the current orbital plane which would result from the PM for each combination of the components $\mu_\alpha \cos\delta$ and μ_δ. The radial grey contour lines illustrate $\cos\theta$ in steps of 0.2. For $\cos\theta > 0.8$ an object's orbital plane is inclined by less than 37° with the VPOS-3, and can therefore be considered to be co-orbiting (best co-orbiting alignment is marked with a thick magenta line). For $\cos\theta < -0.8$, it would be counter-orbiting (best alignment marked with a thin magenta line). The green circular contours indicate the lower limits on the absolute speed of the objects relative to the MW in km s^{-1}. Since their kinematics have not yet been measured, this assumes that they have zero line-of-sight velocity relative to the Galactic standard of rest, resulting in the heliocentric line-of-sight velocities as listed in Table 4.

Table 5. Predicted velocity dispersions for each set of photometric parameters compiled in Table 1.

Name	$\sigma_{\rm Newton}$	$\sigma_{\rm M07}$	$\sigma_{\rm W09}$	$\sigma_{\rm MOND}$	$\frac{\sigma_{\rm MOND}}{\sigma_{\rm Newton}}$	$a_{\rm in}$	$a_{\rm ext}$
	(km s^{-1})					(km^2 s^{-2} kpc^{-1})	
Kim 1	0.14	1.4	1.2	0.18	1.3	110	2280
Ret II	0.38	3.2	1.6	0.68	1.8	120	1160
	0.26	3.0	1.6	0.46	1.8	90	1210
Tri II	0.17	3.1	1.6	0.32	1.9	60	1060
Tuc II	0.24	5.9	2.1	0.56	2.4	40	660
	0.23	7.6	2.3	0.61	2.6	30	540
Hor II	0.21	3.7	1.7	0.61	2.9	60	430
Hor I	0.28	4.2	1.8	0.86	3.1	70	390
	0.38	2.9	1.6	1.11	2.9	130	430
Phe II	0.41	3.1	1.6	1.30	3.2	140	370
	0.30	2.8	1.5	0.89	3.0	110	430
Eri III	0.39	1.8	1.3	1.27	3.2	230	350
	0.25	2.3	1.4	0.78	3.1	120	390
Kim 2	0.24	1.9	1.3	0.79	3.3	130	350
	0.34	1.9	1.3	0.89	2.6	190	550
	0.34	3.4	1.7	1.10	3.2	110	360
Gru I	0.25	4.5	1.9	0.88	3.6	60	290
Pic I	0.36	3.5	1.7	1.35	3.7	110	270
	0.32	3.0	1.6	1.15	3.6	110	290
Hyd II	0.47	4.4	1.9	1.78	3.8	110	270
Peg III	0.27	4.7	1.9	1.30	4.8	70	160
Eri II[a]	1.00	6.7	2.2	3.3	3.3	160	100
	0.68	7.0	2.2	2.8	4.1	100	90

Notes. $\sigma_{\rm Newton}$: predicted velocity dispersion assuming mass-to-light ratio, $M/L = 2$ and that the objects are dark matter free.
$\sigma_{\rm M07}$: predicted velocity dispersion assuming the empirical dark matter halo scaling relation of McGaugh et al. (2007).
$\sigma_{\rm W09}$: predicted velocity dispersion assuming the empirical dark matter halo scaling relation of Walker et al. (2009).
$\sigma_{\rm MOND}$: predicted MONDian velocity dispersions, assuming stellar mass-to-light ratios of $M/L = 2$ for all satellite objects.
$\sigma_{\rm MOND}/\sigma_{\rm Newton}$: ratio of predicted MONDian to predicted Newtonian velocity dispersion.
$a_{\rm in}$: internal MONDian acceleration of the satellite at its half-light radius.
$a_{\rm ext}$: external acceleration acting on the satellite due to the potential of the MW.
[a]Eri II is the only object in the isolated MOND regime, i.e. for which $a_{\rm ext} < a_{\rm in}$.

on these scales (Wolf et al. 2010), while the expected scatter in ΛCDM sub-halo properties is large (Tollerud et al. 2011). Consequently, the observed luminosity should have little predictive power, with the velocity dispersions being essentially stochastic.

There are empirical scaling relations that we can use to anticipate the velocity dispersion of the newly discovered objects. This is done with the scaling relations of McGaugh et al. (2007) and Walker et al. (2009), the results of which are tabulated in Table 5. Walker et al. (2010) showed that the distinct relations of McGaugh et al. (2007) and Walker et al. (2009) were consistent with each other and the data available at the time. However, they are not identical, and give different results when extrapolated into the regime represented by the new objects. We therefore tabulate distinct predictions for each, bearing in mind that these are the extrapolations of empirical scaling relations and are not predictions derived from a specific theory like ΛCDM.

McGaugh et al. (2007) fit the baryon subtracted rotation curves of spiral galaxies to obtain an expression for the rotation velocity due to the dark halo component. Though fit to spirals at larger radii, this relation did a good job[4] of anticipating the common mass scale found for satellite galaxies by Strigari et al. (2008). Assuming $\sigma = V_{\rm h}/\sqrt{3}$ and evaluating at the observed half-light radius (in kpc), the relation of McGaugh et al. (2007) becomes

$$\log\sigma = 1.23 + 0.5\log r_{\rm e}. \quad (2)$$

This anticipates velocity dispersions in the range of 1–7 km s^{-1} (Table 5).

Walker et al. (2009) fit the data for dwarf satellite galaxies to obtain

$$\log\sigma \approx 0.5 + 0.2\log r_{\rm e}. \quad (3)$$

This should be more applicable to the newly discovered objects, if they are indeed dwarf satellites, albeit very small ones. The dependence on size in this regime is rather weaker, anticipating velocity dispersions in the range 1–2.3 km s^{-1} (Table 5). Note that both scaling relations are known to be violated in some cases (Collins et al. 2014).

We may of course have a heterogeneous mix of objects: some might be dwarf satellite galaxies in sub-haloes, while others might simply be star clusters. If so, the different anticipated velocity dispersions should help distinguish these two cases. However, considerable observational care will be required to do so given the small anticipated dispersions.

4.3 MOND

We also tabulate the velocity dispersions predicted by MOND (Milgrom 1983). In this theory, the velocity dispersion should follow from the observed properties of each object, irrespective of whether it is a star cluster or dwarf satellite galaxy. Either way, the physics is the same.

To predict velocity dispersions with MOND, we follow the procedure outlined by McGaugh & Milgrom (2013a). We assume (as done there) that $\Upsilon_\star = 2\,{\rm M}_\odot\,{\rm L}_\odot^{-1}$. This approach has had considerable success in predicting, often a priori, the velocity dispersions of the dwarf satellites of Andromeda and of isolated dwarfs in the LG (McGaugh & Milgrom 2013b; Pawlowski & McGaugh 2014a). A different method employed by Lüghausen, Famaey & Kroupa (2014) has also been successful in predicting the velocity dispersions of the most luminous MW dSph satellites Fornax and Sculptor, but found the measured velocity dispersions of Sextans, Carina and Draco to be higher than predicted.

The velocity dispersion predicted by MOND depends on whether the internal gravitational field $a_{\rm in}$ of an object dominates (the isolated case), or if it is dominated by the external field effect (EFE) of the host galaxy $a_{\rm ex}$. The case that applies depends on the relative strength of the internal and external fields: a system is considered to be in the MOND regime and isolated if $a_{\rm ex} < a_{\rm in} < a_0$, and is in the EFE regime if $a_{\rm in} < a_{\rm ex}$. There are thus two velocity dispersion estimators: that for the isolated case (equation 2 of McGaugh & Milgrom 2013a), and that for the EFE case (equation 3 of McGaugh & Milgrom 2013a).

The internal field depends only on the properties of each object, and is estimated at the half-light radius as in McGaugh & Milgrom (2013a). The external field depends on the total baryonic mass of the MW. For specificity, we adopt the empirical ('bumps

[4] Evaluation of the scaling relation of McGaugh et al. (2007) at 300 pc anticipates $M(<300\,{\rm pc}) = 1.8\times10^7\,{\rm M}_\odot$.

and wiggles') MW model of McGaugh (2008), which provides an estimate of $a_{\rm ex} = V_{\rm MW}^2/R$ at the Galactocentric distance $R = d_{\rm MW}$ of each object. The uncertainty in the circular velocity of the MW at these distances affects the predicted velocity dispersions at the $\pm 0.3\,{\rm km\,s^{-1}}$ level.

The EFE dominates in all but the most distant case: Eri II is the only object in Table 5 in the isolated regime. In some cases, the external field is only marginally dominant. In these cases, neither mass estimator is really adequate, and the velocity dispersion may be slightly underpredicted (Milgrom 1995). In all cases, the enhancement in the velocity dispersion predicted by MOND is rather modest. Typically, it is only a factor of a few above the purely Newtonian (star cluster) case, and is often less than anticipated by the dark halo scaling relations. The many uncertainties of the quantities that go into the prediction are compounded by the potential for systematic errors.

4.4 Challenges to interpretation

Can we hope to observationally distinguish between the various predictions? An accuracy of $\sim 0.1\,{\rm km\,s^{-1}}$ is required to resolve the velocity dispersions anticipated for star clusters. This is certainly possible, if challenging.

The larger concern is systematic uncertainties. For example, are these tiny systems in dynamical equilibrium? If not, we might misinterpret a high velocity dispersion of a dissolving star cluster as the equilibrium dispersion of a dwarf satellite residing in a dark matter sub-halo.

Many of the uncertainties involved in measuring and interpreting velocity dispersions have been discussed by McGaugh & Wolf (2010). We emphasize here just two possible systematics that we fear will make it extremely difficult to distinguish between the various possibilities. One, binary stars may inflate the observed velocity dispersions. Two, the conversion from light to stellar mass is rather fraught for systems containing so few stars.

4.4.1 Binary stars

Some of the individual stars for which velocities are obtained are presumably members of unresolved binaries. Binary stars are themselves in orbit around one another, possibly at speeds comparable to the velocity dispersion expected for the system as a whole. This can inflate the velocity dispersion measured for the system. Binaries can easily contribute enough to the measured velocity dispersion to change the interpretation from one extreme to the other. One can correct for this effect, but it requires the patience of many repeat observations (Simon et al. 2011).

4.4.2 Stellar mass

Another problem when considering ultrafaint dwarfs is the uncertainty in the stellar mass-to-light ratio. Ultrafaint dwarfs are so small that their entire luminosity can be less than that of a single high-mass star. This violates an essential assumption in the estimation of stellar mass-to-light ratios with stellar population models: that there are enough stars to statistically sample all phases of stellar evolution. Indeed, in systems composed of only a few hundred stars, the evolution of a single star up the giant branch will substantially change the luminosity of the entire system without changing its mass. For this reason, all predictions made with an assumed mass-to-light ratio are subject to large uncertainty. This strongly affects the predictions for both purely Newtonian star clusters and MOND.

4.4.3 Ret II, Hor I and Hyd II

Ret II is the first of the objects in Table 5 to have a measured velocity dispersion σ and heliocentric velocity $v_{\rm hel}$. Walker et al. (2015) measure $\sigma = 3.6^{+0.9}_{-0.6}\,{\rm km\,s^{-1}}$ ($v_{\rm hel} = 64.8^{+1.1}_{-1.0}\,{\rm km\,s^{-1}}$), Simon et al. (2015) measure $\sigma = 3.3 \pm 0.7\,{\rm km\,s^{-1}}$ ($v_{\rm hel} = 62.8 \pm 0.5\,{\rm km\,s^{-1}}$) and Koposov et al. (2015b) measure $\sigma = 3.2^{+1.6}_{-0.5}\,{\rm km\,s^{-1}}$ ($v_{\rm hel} = 64.7^{+1.3}_{-0.8}\,{\rm km\,s^{-1}}$). These measurements are nicely consistent, and are clearly too large for a star cluster devoid of dark matter ($0.3\,{\rm km\,s^{-1}}$) or for MOND ($0.5\,{\rm km\,s^{-1}}$). This of course presumes that the system is in dynamical equilibrium, that our guess for the stellar mass-to-light ratio is not far off, and that binary stars contribute $\ll 3\,{\rm km\,s^{-1}}$ in quadrature to the observed velocity dispersion.

We have used the opportunity provided by the independent measurements of Ret II's velocity dispersion to check whether the studies are in mutual agreement or whether systematic errors might be present. This is motivated by the comparison for the Carina dSph by Godwin & Lynden-Bell (1987). We can make a similar comparison for the studies of Walker et al. (2015) and Koposov et al. (2015b), who have 13 Ret II stars in common. The respective velocities measured for these stars are plotted against each other in Fig. 5. We find that the best-fitting line has a slope of 0.79 ± 0.21 and a y-axis intercept of 13.6 ± 13.3 (not counting the outlier with the largest error bars which also disagrees with the systematic velocity of Ret II by almost $15\,{\rm km\,s^{-1}}$ in one of the two studies). Hence, there is indeed a positive correlation between the two velocity sets, which furthermore is consistent with a slope of one. This supports the interpretation that not random errors but indeed the internal

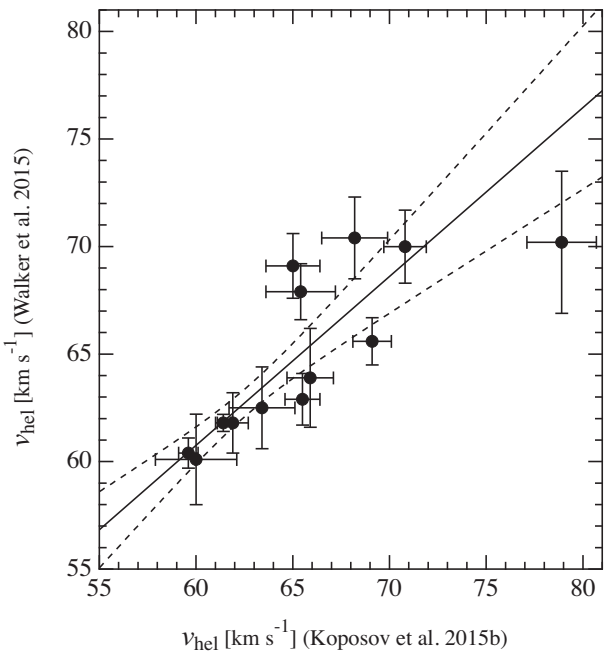

Figure 5. Velocity measurements for those Ret II stars in common between the sets Walker et al. (2015), plotted on the vertical axis, and Koposov et al. (2015b), plotted on the horizontal axis. The data points are plotted with their respective error bars, also shown is the best-fitting line and the upper and lower 2σ confidence bands. We find that the measurements agree well with each other, giving confidence in the reported heliocentric velocity and velocity dispersion for this object.

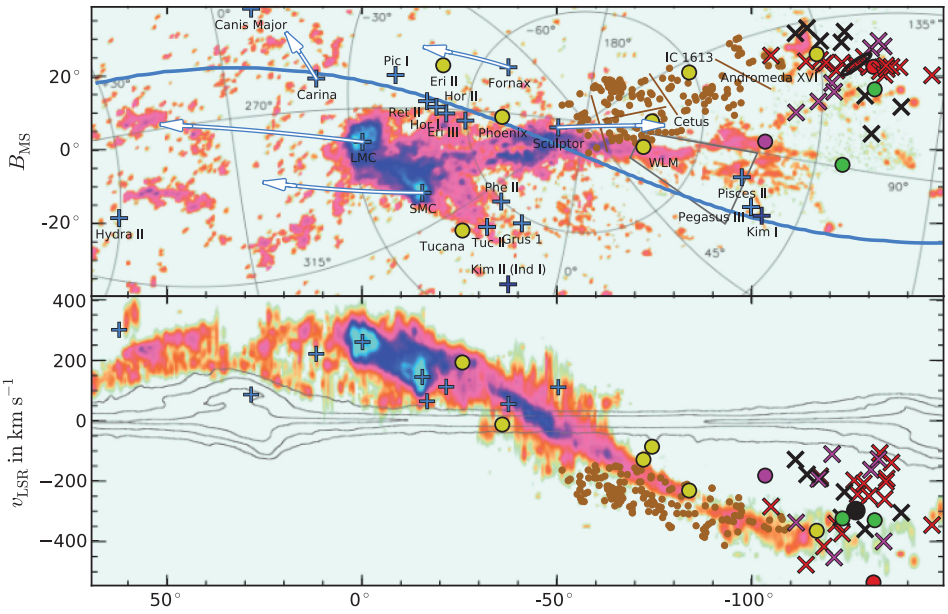

Figure 6. Comparison of the Magellanic Stream (from Nidever et al. 2010) and the LG dwarf galaxies as in fig. 17 of Pawlowski et al. (2013), but updated to include the newly discovered objects and additional information. The upper panel plots positions on the sky in the Magellanic Stream Coordinate (Nidever, Majewski & Burton 2008). The solid blue line indicates the intersection of the best-fit VPOS plane with a sphere of 250 kpc radius. The arrows indicate the current most-likely velocity vectors of the MW satellites LMC, SMC, Fornax, Carina and Sculptor, as compiled in table 2 of Pawlowski & Kroupa (2013). The velocity vectors are represented in position space by converting 5 km s^{-1} to length of 1 kpc and then projected into Magellanic Stream coordinates. As in Fig. 1 the velocity vectors reveal that the satellites move mostly along the plane. The blue plus signs indicate the positions of the MW satellites (dark blue for the two star clusters Kim 1 and 2), yellow dots the positions of the non-satellite dwarf galaxies which are part of a highly flattened plane approximately connecting the MW and M31, and crosses are satellite galaxies of M31 (red for those in the M31 satellite galaxy plane). The black ellipse indicates the position and orientation of M31. The lower panel gives the line-of-sight velocities of the Magellanic Stream and those galaxies for which kinematics are available. See Pawlowski et al. (2013) for further details.

velocity dispersion of the object is a major contributor to the spread in velocities.

Taken at face value, the observed velocity dispersion is consistent with the empirical scaling relation of McGaugh et al. (2007), which anticipates $\sigma = 3$–$4\,\mathrm{km\,s^{-1}}$, depending on whose photometry is employed. This implies a dark matter halo consistent with the near-universal halo found by McGaugh et al. (2007) and Walker et al. (2010). Unfortunately, this empirical dark matter halo is not consistent with ΛCDM (McGaugh et al. 2007), though presumably it can be accommodated by invoking feedback or some other mechanism.

To make matters worse, the universal halo that is successful in the case of Ret II does not work in the cases of the satellites of M31 And XIX, XXI and XXV (Collins et al. 2014). These objects are faint, but have much larger effective radii than the objects under consideration here. Application of equation 2 of McGaugh et al. (2007) anticipates $\sigma > 13\,\mathrm{km\,s^{-1}}$ for these dwarfs of M31, while they are observed to have $\sigma < 5\,\mathrm{km\,s^{-1}}$ (Collins et al. 2014). These objects should be strongly affected by the EFE in MOND, which was unique in accurately predicting their velocity dispersions in advance (McGaugh & Milgrom 2013a,b). We therefore urge caution in interpreting the velocity dispersions of these objects, especially in light of the systematic uncertainties discussed above.

Koposov et al. (2015b) also infer a velocity dispersion for Hor I from five stars of $\sigma = 4.9^{+2.8}_{-0.9}\,\mathrm{km\,s^{-1}}$ ($v_{\mathrm{hel}} = 112.8^{+2.5}_{-2.6}\,\mathrm{km\,s^{-1}}$). This dispersion value exceeds all predictions, but it again comes closest to the prediction using the McGaugh et al. (2007) scaling relation. However, for the reasons discussed above one should be extremely cautious in interpreting these velocity dispersion measurements.

After this manuscript was submitted, Kirby, Simon & Cohen (2015) announced the first spectroscopic measurement of stars in Hyd II. They did not resolve its velocity dispersion, but report an upper limit of $\sigma < 4.5\,\mathrm{km\,s^{-1}}$ (95 per cent confidence), which is consistent with all predictions. Kirby et al. (2015) found a heliocentric velocity for Hyd II of $v_{\mathrm{hel}} = 303.1 \pm 1.4\,\mathrm{km\,s^{-1}}$, which they report to be similar to the Leading arm of the Magellanic Stream. Such a similarity to the velocity of the Magellanic Stream is a general trend for the objects found to lie within the dwarf galaxy planes in the LG (Pawlowski et al. 2013), which is also followed by Ret II and Hor I (see Fig. 6). Unfortunately, the line-of-sight velocity of satellite objects does not provide decisive information on whether it orbits within the VPOS, because this velocity is mostly oriented along the radial component of its position vector from the Galactic centre.

5 DISCUSSION AND CONCLUSIONS

We have compiled a list of 14 recently discovered stellar systems in the vicinity of the MW, many of which are probably MW satellite galaxies. We find that most of these objects align well with the VPOS, which consists of both satellite galaxies and star clusters (Pawlowski et al. 2012). The updated VPOS fit parameters, compiled in Table 2, do not deviate substantially from the previous ones: the rms height is almost unchanged, the orientation preserved to within 9° and the offset from the MW centre is reduced. Assuming that this alignment indicates the objects to be part of a common dynamical structure, as is indicated by the aligned orbital poles of the 11 classical MW satellites (Pawlowski & Kroupa 2013), we predict the PMs of the new satellite objects (see Section 3).

We apply Newtonian and MONDian dynamics and different dark matter halo scaling relations to predict the velocity dispersions of the objects from their photometric properties (see Section 4). These three distinct assumptions result in predictions with only modest differences. For most objects Newtonian dynamics predict velocity dispersion between 0.2 and 0.4 km s^{-1}, the dark matter scaling relations predict velocity dispersions between 1 and 4 km s^{-1} and the MOND predictions lie in between these. This small range of very low velocity dispersions makes it extremely difficult to discriminate between the three cases observationally, which will require very precise measurement and good control of systematic effects such as unresolved binary stars.

Most of the objects are in the Southern hemisphere of the MW, and the majority of them have been discovered in the DES. The survey footprint lies close to the Magellanic Clouds which orbit within the VPOS, such that an alignment with the VPOS might not be unexpected. However, even though the area covered by the DES so far falls close to the VPOS, one would expect the 10 objects discovered in the data to have about 50 per cent larger mean and median offsets from the VPOS if they were drawn from an isotropic distribution confined to the survey footprint. Both mean and median offsets at least as small as observed are rare among such randomized realisations (9 and 4 per cent, respectively). Furthermore, several other objects were discovered elsewhere, away from known concentrations of satellite galaxies, but nevertheless aligned with the VPOS. The fact that the PanSTARRs survey, despite its 3π sky coverage, has so far not resulted in the discovery of a large number satellite galaxies outside of the VPOS provides further hints that even the fainter MW satellites align with the satellite structure which was first discussed almost 40 yr ago by Kunkel & Demers (1976) and Lynden-Bell (1976).

Among the M31 satellite galaxies a similar, and apparently also corotating, plane consisting of about half of the satellite population was found by Ibata et al. (2013). It is aligned with the M31's prominent stellar streams (Hammer et al. 2013), which is reminiscent of the preferential alignment of streams in the MW halo with the VPOS, most prominently the Magellanic Stream. Co-orbiting planes and similar satellite alignments might even be common throughout the Universe (Ibata et al. 2014; Pawlowski & Kroupa 2014; Tully et al. 2015).

The new satellites could prove to be important for the wider picture of dwarf galaxies and the overall dynamics in the LG. The non-satellite LG dwarf galaxies are confined to two highly symmetric and extremely narrow planes (Pawlowski et al. 2013). The dominant of these two planes appears to connect M31 and its satellite galaxy plane with the VPOS around the MW, and agrees in projected position and line-of-sight velocity with the Magellanic Stream (see section 7.4 in Pawlowski et al. 2013 and Fig. 6). The new discoveries are particularly interesting because many lie in the vicinity of the Magellanic Clouds but into the direction of M31, close to the Magellanic Stream. This region was identified as the 'direction of decision' by Pawlowski et al. (2013), because it is where the MW and M31 satellite planes intersect with the dominant plane of non-satellite dwarf galaxies in the LG. Knowledge of the phase-space distribution of objects in this region should help to determine if and how these structures are connected.

ACKNOWLEDGEMENTS

We thank Benoit Famaey, Pavel Kroupa, Federico Lelli, Mario Mateo, Sangmo Tony Sohn and Matthew Walker for useful discussions and comments. HJ acknowledges the support of the Australian Research Council through Discovery Project DP150100862. The contributions of MSP and SSM to this publication were made possible through the support of a grant from the John Templeton Foundation. The opinions expressed in this publication are those of the author and do not necessarily reflect the views of the John Templeton Foundation.

REFERENCES

Bechtol et al., 2015, ApJ, 807, 50 (B15)
Belokurov V. et al., 2006, ApJ, 647, L111
Belokurov V. et al., 2007, ApJ, 654, 897
Belokurov V. et al., 2008, ApJ, 686, L83
Belokurov V. et al., 2009, MNRAS, 397, 1748
Belokurov V. et al., 2010, ApJ, 712, L103
Belokurov V., Irwin M. J., Koposov S. E., Evans N. W., Gonzalez-Solares E., Metcalfe N., Shanks T., 2014, MNRAS, 441, 2124
Collins M. L. M. et al., 2014, ApJ, 783, 7
Deason A. J. et al., 2011, MNRAS, 415, 2607
Gillet N., Ocvirk P., Aubert D., Knebe A., Libeskind N., Yepes G., Gottlöber S., Hoffman Y., 2015, ApJ, 800, 34
Godwin P. J., Lynden-Bell D., 1987, MNRAS, 229, 7P
Grillmair C. J., 2009, ApJ, 693, 1118
Hammer F., Yang Y., Fouquet S., Pawlowski M. S., Kroupa P., Puech M., Flores H., Wang J., 2013, MNRAS, 431, 3543
Ibata R. A. et al., 2013, Nature, 493, 62
Ibata N. G., Ibata R. A., Famaey B., Lewis G. F., 2014, Nature, 511, 563
Jerjen H., 2010, Adv. Astron., 2010, 2
Keller S. C., Mackey D., Da Costa G. S., 2012, ApJ, 744, 57
Kim D., Jerjen H., 2015a, ApJ, 799, 73
Kim D., Jerjen H., 2015b, APJ, 808, 39
Kim D., Jerjen H., Milone A. P., Mackey D., Da Costa G. S., 2015a, ApJ, 803, 63
Kim D., Jerjen H., Mackey D., Da Costa G. S., Milone A. P., 2015b, ApJ, 804, L44
Kirby E. N., Simon J. D., Cohen J. G., 2015, preprint (arXiv:1506.01021)
Koposov S. E., Belokurov V., Torrealba G., Evans N. W., 2015a, ApJ, 805, 130
Koposov S. E. et al., 2015b, preprint (arXiv:1504.07916)
Kroupa P., 1997, New Astron., 2, 139
Kroupa P., Theis C., Boily C. M., 2005, A&A, 431, 517
Kroupa P. et al., 2010, A&A, 523, A32
Kunkel W. E., Demers S., 1976, in Dickens R. J., Perry J. E., Smith F. G., King I. R., eds, Royal Greenwich Observatory Bulletins, Vol. 182, The Galaxy and the Local Group, Herstmonceux, p. 241
Laevens B. P. M. et al., 2014, ApJ, 786, L3
Laevens B. P. M. et al., 2015, ApJ, 802, L18
Law D. R., Majewski S. R., 2010, ApJ, 714, 229
Libeskind N. I., Frenk C. S., Cole S., Helly J. C., Jenkins A., Navarro J. F., Power C., 2005, MNRAS, 363, 146
Libeskind N. I., Frenk C. S., Cole S., Jenkins A., Helly J. C., 2009, MNRAS, 399, 550
Lüghausen F., Famaey B., Kroupa P., 2014, MNRAS, 441, 2497
Lynden-Bell D., 1976, MNRAS, 174, 695
Lynden-Bell D., Lynden-Bell R. M., 1995, MNRAS, 275, 429
McGaugh S. S., 2008, ApJ, 683, 137
McGaugh S., Milgrom M., 2013a, ApJ, 766, 22
McGaugh S., Milgrom M., 2013b, ApJ, 775, 139
McGaugh S. S., Wolf J., 2010, ApJ, 722, 248
McGaugh S. S., de Blok W. J. G., Schombert J. M., Kuzio de Naray R., Kim J. H., 2007, ApJ, 659, 149
Martin N. F. et al., 2015, ApJ, 804, L5
Metz M., Kroupa P., Libeskind N. I., 2008, ApJ, 680, 287
Metz M., Kroupa P., Jerjen H., 2009, MNRAS, 394, 2223
Milgrom M., 1983, ApJ, 270, 365
Milgrom M., 1995, ApJ, 455, 439

Nidever D. L., Majewski S. R., Burton W. B., 2008, ApJ, 679, 432
Nidever D. L., Majewski S. R., Butler Burton W., Nigra L., 2010, ApJ, 723, 1618
Olsen K. A. et al., 2014, in American Astronomical Society Meeting Abstracts, Vol. 223, p. 254.44
Pawlowski M. S., Kroupa P., 2013, MNRAS, 435, 2116
Pawlowski M. S., Kroupa P., 2014, ApJ, 790, 74
Pawlowski M. S., McGaugh S. S., 2014a, MNRAS, 440, 908
Pawlowski M. S., McGaugh S. S., 2014b, ApJ, 789, L24
Pawlowski M. S., Pflamm-Altenburg J., Kroupa P., 2012, MNRAS, 423, 1109
Pawlowski M. S., Kroupa P., Jerjen H., 2013, MNRAS, 435, 1928
Pawlowski M. S. et al., 2014, MNRAS, 442, 2362
Sakamoto T., Hasegawa T., 2006, ApJ, 653, L29
Shaya E. J., Tully R. B., 2013, MNRAS, 436, 2096
Simon J. D. et al., 2011, ApJ, 733, 46
Simon J. D. et al., 2015, ApJ, 808, 95
Strigari L. E., Bullock J. S., Kaplinghat M., Simon J. D., Geha M., Willman B., Walker M. G., 2008, Nature, 454, 1096
The Dark Energy Survey Collaboration 2005, preprint (arXiv:astro-ph/0510346)
Tollerud E. J., Bullock J. S., Graves G. J., Wolf J., 2011, ApJ, 726, 108
Tully R. B., Libeskind N. I., Karachentsev I. D., Karachentseva V. E., Rizzi L., Shaya E. J., 2015, ApJ, 802, L25
Walker M. G., Mateo M., Olszewski E. W., Peñarrubia J., Wyn Evans N., Gilmore G., 2009, ApJ, 704, 1274
Walker M. G., McGaugh S. S., Mateo M., Olszewski E. W., Kuzio de Naray R., 2010, ApJ, 717, L87
Walker M. G., Mateo M., Olszewski E. W., Bailey J. I., Koposov S. E., III, Belokurov V., Wyn Evans N., 2015, ApJ, 808, 108
Walsh S. M., Jerjen H., Willman B., 2007, ApJ, 662, L83
Wang J., Frenk C. S., Cooper A. P., 2013, MNRAS, 429, 1502
Watkins L. L. et al., 2009, MNRAS, 398, 1757
Willman B. et al., 2005a, AJ, 129, 2692
Willman B. et al., 2005b, ApJ, 626, L85
Wolf J., Martinez G. D., Bullock J. S., Kaplinghat M., Geha M., Muñoz R. R., Simon J. D., Avedo F. F., 2010, MNRAS, 406, 1220
York D. G. et al., 2000, AJ, 120, 1579
Zentner A. R., Kravtsov A. V., Gnedin O. Y., Klypin A. A., 2005, ApJ, 629, 219
Zucker D. B. et al., 2006a, ApJ, 643, L103
Zucker D. B. et al., 2006b, ApJ, 650, L41

This paper has been typeset from a TEX/LATEX file prepared by the author.